Optimal Implementation of Miniature Piezoelectric Panel Speakers Using the Taguchi Method and Genetic Algorithm

Mingsian R. Bai
e-mail: msbai@mail.nctu.edu.tw

Yenchih Lu

Department of Mechanical Engineering,
National Chiao-Tung University,
1001 Ta-Hsueh Road, Hsin-Chu 300,
Taiwan, Republic of China

A thin and miniature piezoelectric panel speaker has been developed in this paper. The system is modeled using the energy method in conjunction with the finite element method. The electrical system, mechanical system and acoustic loading are considered in combined fashion. The genetic algorithm (GA) and the Taguchi method are employed to achieve optimal designs with low fundamental frequency and high acoustic output. The designs resulting from the optimization are then implemented and evaluated by experiments. These experiments were carried out on the basis of quantitative and subjective performance measures. The experimental results indicate that the piezoelectric panel speakers are capable of producing comparable acoustic output with significantly less electrical power than the conventional voice-coil panel speakers.
[DOI: 10.1115/1.1759695]

1 Introduction

The 3C industry (Computer, Communication, and Consumer) has recently emerged as one of the most rapidly growing industries of modern days. Commercial products such as personal data assistants (PDAs), mobile phones, MP3 players are currently making their way into the market and everyone's life. From the design point of view, one of the chief concerns of 3C products is miniaturization. This is particularly true for the loudspeaker that is an important component of 3C products. Panel speakers provide a potential solution to meet the requirement of miniaturization [1]. Apart from small size, panel speakers also offer advantages of omni-directional radiation, linearity, insensitivity to room boundary condition and bi-polar radiation [2]. A detailed analysis of the panel speaker can be found in [1]. Despite all the advantages, panel speakers suffer from two drawbacks that limit their use in practical 3C applications. First, the exciter for a panel speaker is traditionally the voice-coil type and could reach only approximately 2 mm thickness, which is still too thick to apply in many 3C products such as mobile phones. Second, the electro-acoustic efficiency driven by the voice-coil exciters was found to be quite low [1], which presents problem of power consumption to mobile electronic products. These physical limitations associated with the conventional voice-coil exciters hence motivate the present development of an alternative way of excitation for panel speakers.

In this paper, panel speakers excited by piezoelectric ceramics are proposed, in an attempt to overcome the problems encountered in voice-coil exciters [3]. Relatively high efficiency of piezoelectric material makes the piezoelectric panel speaker an ideal device for many battery-powered products. Although the piezoelectric panel speakers have been around for some time, these devices mainly exist in the forms of narrowband acoustic radiators such as buzzers, sounders, sirens, etc., where sound quality is generally not of the major concern. By contrast, this work seeks to meet the requirements of quality loudspeakers for speech and music rendering. To this end, optimization techniques are utilized to achieve practical designs with minimum fundamental frequency and the maximum sound pressure output.

This paper is organized as follows. First, the dynamic model of the piezoelectric speaker was derived using the energy method and the finite element method (FEM). Unlike Ref. [1], the electrical system, mechanical system and acoustic loading are considered as a coupled system during dynamic modeling. This is important for a light structure like a panel speaker, especially for low frequencies where acoustic mass loading is not negligible. Second, the Taguchi method and the genetic algorithm (GA) are employed to optimize the speaker design. The Taguchi method is used for a preliminary search, whereas the GA is used to ''fine tune'' the design parameters. Designs resulting from the optimization are then implemented and evaluated experimentally. In order to evaluate the speaker performance, quantitative measures as well as subjective indices are measured and summarized.

2 Modeling of Piezoelectric Panel Speakers

In the following derivation of equation of motion for the piezoelectric panel speaker, the electrical system, mechanical system and the acoustic loading are modeled as a coupled system.

2.1 Energy Method and Variation Principle. The basic structure of a piezoelectric panel speaker consists of a rectangular piezoelectric ceramic plate and a thin rectangular panel of length L_p and width W_p, as shown in Fig. 1. Let the lateral displacement field be $w=w(x,y,t)$. The bending strain energy of the panel is given by [4]

$$U_p=\frac{1}{2}D_p\int_0^{L_p}\int_0^{W_p}[w_{xx}^2+w_{yy}^2+2\upsilon w_{xx}w_{yy}+2(1-\upsilon)w_{xy}^2]dxdy, \tag{1}$$

where $D_p=E_ph_p^3/12(1-\upsilon^2)$ is the bending stiffness of the panel, h_p is the thickness of the panel, E_p is the Young's modulus of the panel, and υ is the Poisson's ratio of the panel. The subscript ''xx'' denotes the second partial derivative with respect to the space coordinate x; similar rule applies to the other variables. It should be clear from the context, where all subscripts in the following equations that are not in the definition of the variable should be interpreted as differentiation with respect to the variable. In addition, the kinetic energy of the panel is given by

$$T_p=\frac{1}{2}\int_0^{L_p}\int_0^{W_p}\rho_p w_t^2 dxdy, \tag{2}$$

Contributed by the Technical Committee on Vibration and Sound for publication in the JOURNAL OF VIBRATION AND ACOUSTICS. Manuscript received August 2003; Revised January 2004. Associate Editor: R. F. Keltie.

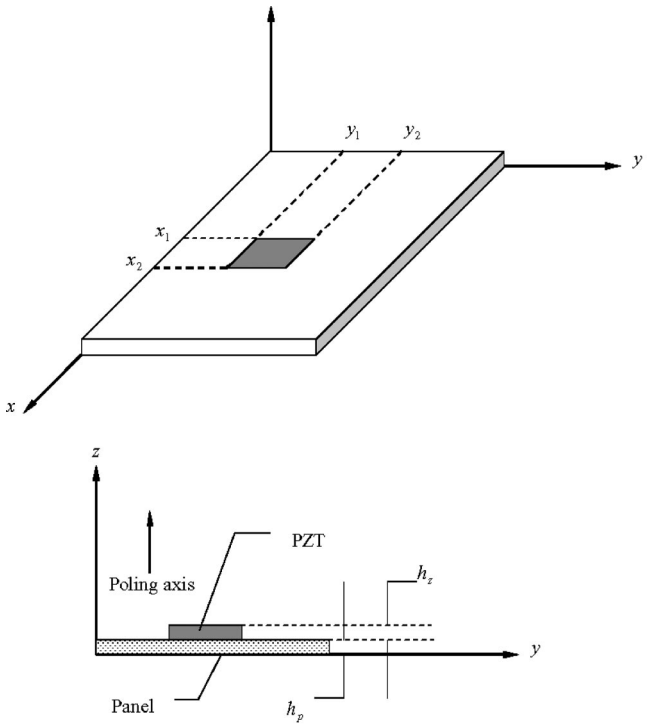

Fig. 1 Schematic diagram of the piezoelectric panel speaker

where ρ_p is the area density of the panel and the subscript "t" denotes the first partial derivative with respect to the time variable t. Similarly, the kinetic energy of the PZT plate is given by

$$T_z=\frac{1}{2}\int_{x_1}^{x_2}\int_{y_1}^{y_2}\rho_z w_t^2 dxdy, \tag{3}$$

where ρ_z is the area density of the PZT plate.

In this paper, the piezoelectric equations are based on the h-form and the PZT plate is a hexagonal crystal class (6mm). The h-form of the linear piezoelectric equations is written as

$$\begin{bmatrix} T_1 \\ T_2 \\ T_6 \\ E_3 \end{bmatrix} = \begin{bmatrix} c_{11}^D & c_{12}^D & 0 & -h_{31} \\ c_{12}^D & c_{11}^D & 0 & -h_{31} \\ 0 & 0 & c_{66}^D & 0 \\ -h_{31} & -h_{31} & 0 & \beta_{33}^S \end{bmatrix} \begin{bmatrix} S_1 \\ S_2 \\ S_6 \\ D_3 \end{bmatrix}, \tag{4}$$

where T is the stress, S is the strain, D is the dielectric displacement, E is the field strength, h is the piezoelectric voltage constant, c^D is the elastic stiffness under the condition of constant dielectric displacement, and β^S is the permittivity under the condition of constant strain.

By the Kirchhoff plate theory, it is assumed that the transverse shear deformation is zero and angles of rotation are small. The strains are assumed to follow

$$S_1=-zw_{xx}, \quad S_2=-zw_{yy}, \quad S_6=-2zw_{xy}, \tag{5}$$

By Eqs. (4) and (5), the internal energy of the PZT plate can be written as [5]

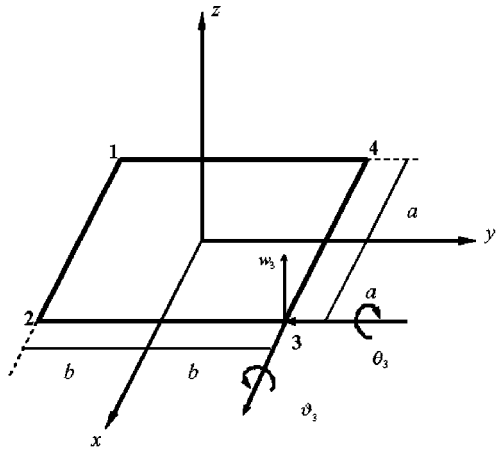

(a)

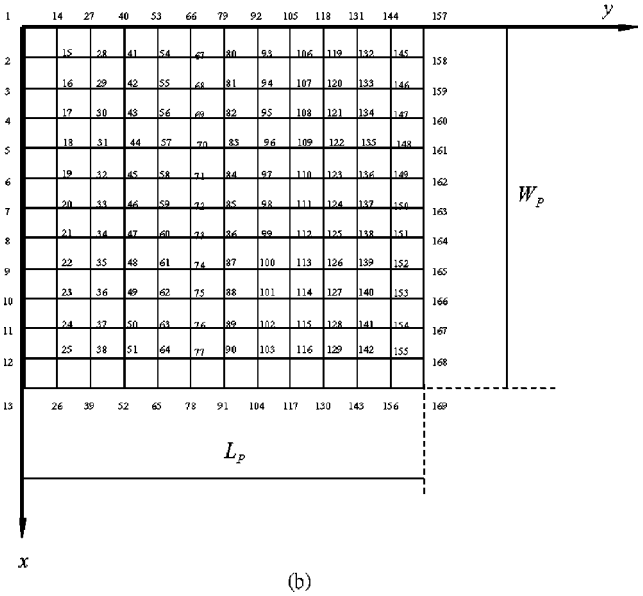

(b)

Fig. 2 FEM mesh structure for modeling the piezoelectric panel speaker (*a*) a 12-dof plate element, with dofs indicated at node 3 (*b*) complete mesh with 144 elements for the piezoelectric speaker

$$\begin{aligned} U_z=&\frac{1}{2}\int_{h_p}^{h}\int_{y_1}^{y_2}\int_{x_1}^{x_2}(T_1S_1+T_2S_2+T_6S_6+E_3D_3)dxdydz \\ =&\frac{c_{11}^D(h^3-h_p^3)}{6}\int_{y_1}^{y_2}\int_{x_1}^{x_2}(w_{xx}^2+w_{yy}^2)dxdy \\ &+\frac{c_{12}^D(h^3-h_p^3)}{3}\int_{y_1}^{y_2}\int_{x_1}^{x_2}w_{xx}w_{yy}dxdy \\ &+\frac{h_{31}D_3(h^2-h_p^2)}{2}\int_{y_1}^{y_2}\int_{x_1}^{x_2}(w_{xx}+w_{yy})dxdy \\ &+\frac{\beta_{33}^S D_3^2(h-h_p)}{2}\int_{y_1}^{y_2}\int_{x_1}^{x_2}dxdy \\ &-\frac{2c_{66}^D(h^3-h_p^3)}{3}\int_{y_1}^{y_2}\int_{x_1}^{x_2}w_{xy}^2dxdy, \end{aligned} \tag{6}$$

where $h=h_p+h_z$.

On the other hand, the virtual work done by the non-inertial forces and the external voltage can be expressed as

$$\delta W_{vir}=\int_{y_1}^{y_2}\int_{x_1}^{x_2} f(x,y,t)\,\delta w\,dx\,dy+\int_{y_1}^{y_2}\int_{x_1}^{x_2} v_z(t)\,\delta D_3\,dx\,dy, \tag{7}$$

where $f(x,y,t)$ denotes the external force on the surface and $v_z(t)$ denotes the voltage applied to the PZT.

2.2 FEM Model. Since the piezoelectric ceramic and the vibrating panel are very thin, two-dimensional finite elements should suffice in the subsequent analysis. In the FEM formulation, the lateral displacement w of an element is interpolated by third degree polynomials of physical coordinates [6]

$$w=\mathbf{xa}, \tag{8}$$

where

$$\mathbf{x}=[1,x,y,x^2,xy,y^2,x^3,x^2y,xy^2,y^3,x^3y,xy^3]$$

is the physical coordinate vector and

$$\mathbf{a}=[a_1,a_2,a_3,a_4,a_5,a_6,a_7,a_8,a_9,a_{10},a_{11},a_{12}]^T$$

is the coefficient vector to be determined. Assume the element is of length $2b$ and width $2a$. The nodal degree of freedoms (dof) consist of lateral deflections w_i and rotations $\partial w_i/\partial x=\theta_i$ and $\partial w_i/\partial y=\vartheta_i$, $i=1, 2, 3, 4$, as shown in Fig. 2(*a*). The dofs of the element are grouped into a vector

$$\mathbf{d}=[w_1,\theta_1,\vartheta_1,w_2,\theta_2,\vartheta_2,w_3,\theta_3,\vartheta_3,w_4,\theta_4,\vartheta_4]^T$$

The mesh configuration of finite elements is shown in Fig. 2(*b*). To express the $a_j, j=1,2,\ldots,12$ in terms of the physical ordinates and the slopes at four corners, $(x,y)=(-a,-b)$, $(x,y)=(a,-b)$, $(x,y)=(a,b)$ and $(x,y)=(-a,b)$, we make the following substitutions

$$w=w_1,\quad \partial w/\partial x=\theta_1,\quad \partial w/\partial y=\vartheta_1 \quad \text{at } (x,y)=(-a,-b),$$

$$w=w_2,\quad \partial w/\partial x=\theta_2,\quad \partial w/\partial y=\vartheta_2 \quad \text{at } (x,y)=(a,-b),$$

$$w=w_3,\quad \partial w/\partial x=\theta_3,\quad \partial w/\partial y=\vartheta_3 \quad \text{at } (x,y)=(a,b),$$

$$w=w_4,\quad \partial w/\partial x=\theta_4,\quad \partial w/\partial y=\vartheta_4 \quad \text{at } (x,y)=(-a,b)$$

into Eq. (8) and obtain

$$\begin{bmatrix} w_1\\ \theta_1\\ \vartheta_1\\ \vdots\\ w_4\\ \theta_4\\ \vartheta_4 \end{bmatrix}=\begin{bmatrix} 1 & -a & -b & a^2 & ab & b^2 & -a^3 & -a^2b & -ab^2 & -b^3 & a^3b & ab^3\\ 0 & 1 & 0 & -2a & -b & 0 & 3a^2 & 2ab & b^2 & 0 & -3a^2b & -b^3\\ 0 & 0 & 1 & 0 & -a & -2b & 0 & a^2 & 2ab & 3b^2 & -a^3 & -3ab^2\\ & \vdots & & & & & \vdots & & & & \vdots & \\ 1 & -a & b & a^2 & -ab & b^2 & -a^3 & a^2b & -ab^2 & b^3 & -a^3b & -ab^3\\ 0 & 1 & 0 & -2a & b & 0 & 3a^2 & -2ab & b^2 & 0 & 3a^2b & b^3\\ 0 & 0 & 1 & 0 & -a & 2b & 0 & a^2 & -2ab & 3b^2 & -a^3 & -3ab^3 \end{bmatrix}\begin{bmatrix} a_1\\ a_2\\ a_3\\ \vdots\\ a_{10}\\ a_{11}\\ a_{12} \end{bmatrix}$$

or in matrix notation

$$\mathbf{d}=\mathbf{Ta}$$

Therefore,

$$\mathbf{a}=\mathbf{T}^{-1}\mathbf{d} \tag{9}$$

With Eq. (9) inserted into (8), the lateral displacement w of the element can be rewritten as

$$w=\mathbf{xT}^{-1}\mathbf{d} \tag{10}$$

On the other hand, the displacement field w can also be interpolated over an element using the shape function matrix $\mathbf{N}$

$$w=\mathbf{Nd} \tag{11}$$

which identifies the shape function matrix $\mathbf{N}$ as

$$\mathbf{N}=\mathbf{xT}^{-1} \tag{12}$$

Substituting Eq. (11) into (6) and assembling the element stiffness matrices into the global matrix, the internal energy of the PZT plate can be expressed as

$$U_z=I_1\mathbf{D}^T\mathbf{K}_1\mathbf{D}+I_2\mathbf{D}^T\mathbf{K}_2\mathbf{D}+I_3\mathbf{D}^T\mathbf{K}_3\mathbf{D}+I_4\mathbf{D}^T\mathbf{K}_4q+I_5q^2 - I_6\mathbf{D}^T\mathbf{K}_6\mathbf{D}, \tag{13}$$

where

$$I_1=c_{11}^D(h^3-h_p^3)/6,\ I_2=c_{11}^D(h^3-h_p^3)/6,\ I_3=c_{12}^D(h^3-h_p^3)/3,$$

$$I_4=h_{31}(h^2-h_p^2)/2A_e,\quad I_5=\beta_{33}(h-h_p)/2A_e,$$

$$I_6=2c_{66}^D(h^3-h_p^3)/3,$$

$$\mathbf{K}_1=\sum_{n=1}^{s}\int_{-b}^{b}\int_{-a}^{a}\mathbf{B}_1^T\mathbf{B}_1\,dx\,dy,\quad w_{xx}=\mathbf{B}_1\mathbf{d},\quad \mathbf{B}_1=\partial^2\mathbf{N}/\partial x^2,$$

$$\mathbf{K}_2=\sum_{n=1}^{s}\int_{-b}^{b}\int_{-a}^{a}\mathbf{B}_2^T\mathbf{B}_2\,dx\,dy,\quad w_{yy}=\mathbf{B}_2\mathbf{d},\quad \mathbf{B}_2=\partial^2\mathbf{N}/\partial y^2,$$

$$\mathbf{K}_3=\sum_{n=1}^{s}\int_{-b}^{b}\int_{-a}^{a}\mathbf{B}_1^T\mathbf{B}_2\,dx\,dy,$$

$$\mathbf{K}_4=\sum_{n=1}^{s}\int_{-b}^{b}\int_{-a}^{a}(\mathbf{B}_1+\mathbf{B}_2)^T\,dx\,dy$$

$$\mathbf{K}_6=\sum_{n=1}^{s}\int_{-b}^{b}\int_{-a}^{a}\mathbf{B}_5^T\mathbf{B}_5\,dx\,dy,\quad w_{xy}=\mathbf{B}_5\mathbf{d},$$

$$\mathbf{B}_5=\partial^2\mathbf{N}/\partial x\,\partial y,\mathbf{D}=\sum_{n=1}^{s}\mathbf{d},$$

where s is the total number of elements, $D_3=q/A_e$, q is the electric charge on the electrodes, A_e is the area of each element and $\mathbf{D}$ is the global dof vector.

By the same token, the strain energy and kinetic energy of the vibrating panel can be expressed as

$$U_p=\tfrac{1}{2}\mathbf{D}^T\mathbf{K}_7\mathbf{D}, \tag{14}$$

$$T_p = \tfrac{1}{2}\rho_p \dot{\mathbf{D}}^T \mathbf{K}_8 \dot{\mathbf{D}}, \tag{15}$$

In addition, the kinetic energy of the PZT plate can be written as

$$T_z = \tfrac{1}{2}\rho_z \dot{\mathbf{D}}^T \mathbf{K}_9 \dot{\mathbf{D}}, \tag{16}$$

The virtual work done by the external force and electric charge is expressed as

$$\delta W_{vir} = \delta \mathbf{D}^T \mathbf{f} + \mathbf{v}_z \delta q, \tag{17}$$

The relevant symbols in Eqs. (14)–(17) are defined as follows

$$\dot{\mathbf{D}} = d\mathbf{D}/dt, \mathbf{K}_7 = \int_{-b}^{b}\int_{-a}^{a} \mathbf{B}_7^T \mathbf{D}_K \mathbf{B}_7 dxdy, \quad \mathbf{B}_7^T = [\mathbf{B}_1 \quad \mathbf{B}_2 \quad 2\mathbf{B}_5],$$

$$\mathbf{D}_K = \begin{bmatrix} D_p & \upsilon D_p & 0 \\ \upsilon D_p & D_p & 0 \\ 0 & 0 & \dfrac{(1-\upsilon)}{2} D_p \end{bmatrix},$$

$$\mathbf{K}_8 = \int_{-b}^{b}\int_{-a}^{a} \mathbf{N}^T \mathbf{N} dxdy, \mathbf{K}_9 = \int_{-b}^{b}\int_{-a}^{a} \mathbf{N}^T \mathbf{N} dxdy,$$

$$\mathbf{f} = \sum_{n=1}^{s} \int_{-b}^{b}\int_{-a}^{a} f(x,y,t) dxdy, \mathbf{v}_z = \frac{1}{A_e}\sum_{n=1}^{s} \int_{-b}^{b}\int_{-a}^{a} v_z(t) dxdy$$

2.3 The Lagrange's Equation. The dynamic model of the piezoelectric panel speaker can be obtained by substituting the preceding energy terms into the Lagrange's equation

$$\begin{cases} \dfrac{d}{dt}\left(\dfrac{\partial L}{\partial \dot{\mathbf{D}}^T}\right) - \dfrac{\partial L}{\partial \mathbf{D}^T} = \mathbf{f} \\ -\dfrac{\partial L}{\partial q} = \mathbf{v}_z \end{cases}, \tag{18}$$

where the *Lagrangian* $L = U_p + U_z - T_p - T_z$. With some manipulations, the dynamic model of a piezoelectric panel speaker can be shown as

$$\begin{cases} [(\rho_p \mathbf{K}_8 + \rho_z \mathbf{K}_9)\omega^2 - 2I_1\mathbf{K}_1 - 2I_2\mathbf{K}_2 - 2I_3\mathbf{K}_3 + 2I_6\mathbf{K}_6 - \mathbf{K}_7]\mathbf{D} - I_4\mathbf{K}_4 q = \mathbf{f} \\ -I_4\mathbf{K}_4^T\mathbf{D} - 2I_5 q = \mathbf{v}_z \end{cases}, \tag{19}$$

where $\dot{\mathbf{D}} = \mathbf{v} = j\omega\mathbf{D}$, $\ddot{\mathbf{D}} = -\omega^2\mathbf{D}$.

2.4 Acoustic Loading. Although the acoustic loading is a distributed type of external force, an analysis can still be carried out, using the following discrete approximation. Let **p** and **v** be the pressure vector and velocity vector measured at discrete points on the structure surface. In physical coordinates, **p** and **v** can be related with a radiation impedance matrix **Z** [7]

$$\mathbf{p} = \mathbf{Z}\mathbf{v} \tag{20}$$

For a baffled planar radiator, the matrix **Z** can be approximated as

$$\mathbf{Z} = \rho_a c_s \begin{bmatrix} 1 - e^{-jk\sqrt{A_e/\pi}} & \dfrac{jkA_e}{2\pi}\dfrac{e^{-jkr_{12}}}{r_{12}} & \cdots & \dfrac{jkA_e}{2\pi}\dfrac{e^{-jkr_{1n}}}{r_{1n}} \\ \dfrac{jkA_e}{2\pi}\dfrac{e^{-jkr_{21}}}{r_{21}} & 1 - e^{-jk\sqrt{A_e/\pi}} & \cdots & \vdots \\ \vdots & \vdots & \ddots & \vdots \\ \dfrac{jkA_e}{2\pi}\dfrac{e^{-jkr_{m1}}}{r_{m1}} & \cdots & \cdots & 1 - e^{-jk\sqrt{A_e/\pi}} \end{bmatrix}, \tag{21}$$

where ρ_a is the air density, c_s is the sound speed, k is the wave number, r_{mn} is the distance between the nodes m and n ($r_{mn} = r_{nm}$, $1 \leqslant m,n \leqslant N$). Thus, the external force vector **f** is simply the pressure multiplied by the effective element area A_e

$$\mathbf{f} = A_e\mathbf{p} = A_e\mathbf{Z}\mathbf{v} = j\omega A_e \mathbf{Z}\mathbf{D} \tag{22}$$

2.5 Proportional Damping. In order to incorporate the damping mechanism into the system, *proportional damping* [8] is assumed in this paper for simplicity. That is, the damping matrix **C** is given by

$$\mathbf{C} = \alpha\mathbf{M}_d + \beta\mathbf{K}_d, \tag{23}$$

where α and β are constants. In our problem, $100 < \alpha < 250$ and $5\times10^{-7} < \beta < 1.5\times10^{-6}$. $\mathbf{M}_d$ and $\mathbf{K}_d$ denote the mass matrix and stiffness matrix, respectively, and are calculated according to the following equations

$$\mathbf{M}_d = 2I_5(\rho_l\mathbf{K}_8 + \rho_z\mathbf{K}_9),$$

$$\mathbf{K}_d = 2I_5(-2I_1\mathbf{K}_1 - 2I_2\mathbf{K}_2 - 2I_3\mathbf{K}_3 + 2I_6\mathbf{K}_6 - \mathbf{K}_7) + I_4\mathbf{K}_4\mathbf{K}_4^T$$

With the damping matrix **C** added to Eq. (19), the displacement vector **D** can be solved as follows

$$\mathbf{D} = -I_4(\mathbf{K} + j\omega\mathbf{C})^{-1}\mathbf{K}_4\mathbf{v}_z, \tag{24}$$

where

$$\mathbf{K} = \{2I_5[(\rho_p\mathbf{K}_8 + \rho_z\mathbf{K}_9)\omega^2 - 2I_1\mathbf{K}_1 - 2I_2\mathbf{K}_2 - 2I_3\mathbf{K}_3 + 2I_6\mathbf{K}_6 - \mathbf{K}_7 - j\omega A_e\mathbf{Z}] + I_4\mathbf{K}_4\mathbf{K}_4^T\}$$

2.6 Radiated Sound Pressure. Now that the surface displacements have been obtained from Eq. (24), the radiated sound pressure at any field point can be calculated using the following matrix Eq. [7]

$$\mathbf{p}_{far} = \mathbf{E}\mathbf{v}, \tag{25}$$

where $\mathbf{p}_{far}$ is the radiated sound pressure vector, **v** is the surface velocity vector that can be calculated by differentiating displacements obtained from Eq. (24), and **E** is the propagation matrix. For a baffled planar radiator, the propagation matrix **E** can be approximated as

$$\mathbf{E} = j\frac{\rho_0 c_s k A_e}{2\pi} \begin{bmatrix} \dfrac{e^{-jkr_{11}}}{r_{11}} & \dfrac{e^{-jkr_{12}}}{r_{12}} & \cdots & \dfrac{e^{-jkr_{1n}}}{r_{1n}} \\ \dfrac{e^{-jkr_{21}}}{r_{21}} & \dfrac{e^{-jkr_{22}}}{r_{22}} & \cdots & \dfrac{e^{-jkr_{2n}}}{r_{11}} \\ \vdots & \vdots & \ddots & \vdots \\ \dfrac{e^{-jkr_{m1}}}{r_{m1}} & \dfrac{e^{-jkr_{m2}}}{r_{m2}} & \cdots & \dfrac{e^{-jkr_{mn}}}{r_{mn}} \end{bmatrix}, \tag{26}$$

where A_e is the effective element area and r_{mn} is the distance between the element n and the field point m.

Table 1 The first set of optimal parameters obtained using the Taguchi method. The upper part is the $L_8(4\times2^4)$ orthogonal array

	Factor				
Run	A	B	C	D	E
1	1	1	1	1	1
2	1	2	2	2	2
3	2	1	1	2	2
4	2	2	2	1	1
5	3	1	2	1	2
6	3	2	1	2	1
7	4	1	2	2	1
8	4	2	1	1	2

	Level			
Factor	The f_t of each level			
A (PZT position)	1	2	3	4
	57	55	31	29
	25.0096	40.0299	37.1684	6.5007
B (Young's modulus	6 GPa	60 GPa		
of Panel material)	29.5755	24.7788		
C (PZT shape)	1:1	1:2		
	45.0582	9.2960		
D (PZT Area:	1:9	1:4		
Panel Area)	10.1983	44.1560		
E (Suspension)	Simply supported	Spring supported		
	26.1170	28.2373		

Run	1	2	3	4	5	6	7	8
f_0 (Hz)	150	200	100	1000	200	150	500	300
p_{avg} (dB)	86.2292	87.1675	91.8806	78.6667	75.2395	94.2445	84.8024	79.1988

3 Optimal Design of Piezoelectric Panel Speakers

3.1 Taguchi Method. The Taguchi method is an experimental design procedure well suited for examining a multi-factor design problem using a minimum number of observations [9]. A general Taguchi procedure provides three kinds of functions: system design, parameter design, and tolerance design. For our problem at hand, we focus primarily on parameter design. The goal of parameter design is to pin-point the optimal configuration of a system according to a cost function. The cost function we wish to maximize in our problem is

$$f_t=\frac{10^{(p_{avg}-94)/20}}{f_0}\times 10{,}000, \tag{27}$$

where f_0 is the first resonance frequency with sound pressure level greater than 40 dB, p_{avg} is the average of magnitude of sound pressure level (in dB) above the frequency f_0.

To illustrate the Taguchi procedure, we start with a $L_8(4\times2^4)$ orthogonal array shown in Table 1. The notation $L_8(4\times2^4)$ means that the experimental design requires eight observations and five factors: the first one at four levels and the other four at two levels. In Table 1, the numbers $1\sim2$ indicate the corresponding levels of a factor. The values of cost function are calculated according to the orthogonal array at the upper part of Table 1. For example, the value of cost function corresponding to the second level of factor B (Young's modulus of panel material) is the algebraic average of the 4 occurrences of level 2 among the 8 runs:

$$f_{Bt}=\frac{f_{Bt2}+f_{Bt4}+f_{Bt6}+f_{Bt8}}{4}=24.7788,$$

Similar procedure applies to the other entries of cost function calculation. The larger values of the cost function correspond to better performances achieved by a particular combination of parameter.

A preliminary search of optimal design of the panel speaker is summarized in Tables 1 and 2. In each table, the dimensions of the panel are 42 mm$\times$84 mm$\times$0.1 mm. The parameters considered in the design are the PZT position, Young's modulus of panel material, PZT shape, ratio of PZT area versus panel area, and suspension. Various levels of each parameter are examined in these tables. Because there are many levels of PZT positions (factor A), we subdivided the cases into 3 tables. The fundamental frequency f_0 of Run 4 appears somewhat high because, according to the setting in Table 1, the panel speaker in Run 4 is made of stiffer material (the Young's modulus$=$60 GPa) and is simply supported (as opposed to the compliant support in the other case). Higher damping results in larger cost function. Damping does help the acoustic output at least at the nearfield. From the results, we also found that large values of cost function occurred when the PZT position is between nodes 31 and 68, Young's modulus of panel material is between 0.6 and 600 GPa, and the PZT shape is square. As indicated by the results obtained using the Taguchi procedure, the ratio of PZT area versus the panel area should be as large as possible. This is due to the fact that the cost function, with a modal analysis based on the fundamental mode, can be shown to be a monotonically increasing function of area, and a monotonically decreasing function of thickness. Hence, the area of the PZT is no longer considered in the following GA optimization. The type of suspension appeared inconsequential. Next, we decided to ''fine-tune'' only two design parameters, the Young's modulus of panel and the PZT position.

3.2 The Genetic Algorithm (GA). GA is one of the powerful methods in solving optimization problems [10]. Analogous to the natural selection of evolution, a typical GA session involves three basic genetic operations, *reproduction*, *crossover* and *mutation*. These operations are used in each generation to generate new population with different *chromosomes* in which the design parameters are encoded. With evolution of sufficient number of generations, the optimal solution corresponding to the largest *fitness function* can be found. The principal difference between GA and other optimization methods is that GA operates on multiple starting points in random fashion, making it less susceptible to the problem of local optima.

The first step of GA is to encode the design parameters into binary strings called chromosomes. The resolution of a parameter space is determined by the formula

Table 2 The second and third sets of optimal parameters obtained using the Taguchi method

Factor	Level			
	The f_t of each level			
A (PZT position)	1	2	3	4
	57	56	81	43
	19.6073	42.2398	24.6517	36.0920
B (Young's modulus	6 GPa	600 GPa		
of Panel material)	32.4006	28.8948		
C (PZT shape)	1:1	1:3		
	59.0211	2.2743		
D (PZT Area:	36:144	49:144		
Panel Area)	29.1084	32.1870		
E (Suspension)	Simply supported	Spring supported		
	20.5801	40.7153		

Run	1	2	3	4	5	6	7	8
f_0 (Hz)	150	400	100	1200	250	150	900	150
p_{avg} (dB)	89.1464	66.7733	92.4828	69.6750	78.2962	90.1393	72.5775	94.5764

Factor	Level			
	The f_t of each level			
A (PZT position)	1	2	3	4
	33	32	68	69
	26.7669	49.9882	57.3610	23.7653
B (Young's modulus	6 GPa	0.6 GPa		
of Panel material)	37.9973	40.9434		
C (PZT shape)	1:1	1:4		
	77.8504	1.0902		
D (PZT Area:	49:144	64:144		
Panel Area)	25.2752	53.6655		
E (Suspension)	Simply supported	Spring supported		
	41.9260	37.0147		

Run	1	2	3	4	5	6	7	8
f_0 (Hz)	100	150	100	800	750	50	1050	150
p_{avg} (dB)	88.3091	61.6007	93.8806	74.6149	70.1613	89.1072	69.4322	90.9578

$$R_{E_p} = \frac{E_p^U - E_p^L}{2^{l_p} - 1}, \tag{28}$$

where E_p^U and E_p^L are the upper and lower limits of the parameter to encode, e.g., Young's modulus of the panel. If $1\ \text{GPa} \leqslant E_p \leqslant 200$ GPa and the desired resolution is $R_{E_p} = 0.1945$, $l_p = 10$ and if $E_p = 2.7507$, the chromosome is encoded as [0000001010].

The Fitness function serves as the performance index for GA. A chromosome with high fitness has higher probability of reproducing offspring in the next generation. Our goal of the GA optimization is to minimize the fundamental frequency f_0 and to maximize the average sound pressure level p_{avg} in the bandwidth 12.8 kHz, as shown in Fig. 3(a). The same fitness function defined in Eq. (27) is used in the optimization procedure.

Reproduction directs the search of GA towards the best individuals. The reproduction probability of the chromosome is determined by the fitness function. The chromosome of the present population is reproduced in the next generation according to the probability

$$S_i = \frac{f_{ci}}{\Sigma_{k=1}^{P_l} f_{ck}}, \tag{29}$$

where f_{ci} is the fitness function of the i^{th} chromosome and P_l is the population size. For instance, there are four chromosomes, $c_1 \sim c_4$, in the 0^{th} generation with fitness functions 30, 9, 68 and 52. Substituting these values into Eq. (29) leads to the reproduction probabilities $S_1 = 0.1887$, $S_2 = 0.0566$, $S_3 = 0.4277$, $S_4 = 0.3271$, respectively. These probabilities are then concatenated into a real line, as shown in Fig. 3(b). Clearly, the chromosomes c_3 and c_4 are the most likely to reproduce in the next generation. In the present population, four random numbers between 0 and 1 are generated. For example, if the four random numbers are 0.3644, 0.1835, 0.9237 and 0.4427, the chromosomes survive to next generation will be c_3, c_1, c_4 and c_3, respectively.

Crossover serves to exchange the information of chromosomes via a probabilistic process in the mating pool. First, the crossover ratio C_r is defined. In general, $0.8 \leqslant C_r \leqslant 1$ and we choose $C_r = 0.9$. Two chromosomes in the present population are selected randomly. Second, an arbitrary splice point at the chromosomes is selected. Third, the chromosomes codes after the splice point are interchanged. To illustrate, assume two chromosomes c_1 and c_2 with the splice point at the third bit: $c_1 = 011_\Delta 0111$ and $c_2 = 101_\Delta 1001$. After crossover, two new chromosomes are generated: $\tilde{c}_1 = 011_\Delta 1001$ and $\tilde{c}_2 = 101_\Delta 0111$.

However, the gene will become increasingly homogeneous if one gene begins to dominate after several generations and eventually results in premature convergence. To alleviate this problem, mutation is introduced into the GA procedure. Let the mutation ratio be M_r. In general, $0 \leqslant M_r \leqslant 0.01$ and we choose $M_r = 0.01$. The mutation point is determined randomly. Mutation is done by alternating the gene from zero to one, and vice versa. For example, a chromosome c_1 with the mutation point at the third bit is $c_1 = 101_\Delta 10100$. After mutation, the chromosome becomes $\tilde{c}_1 = 100_\Delta 10100$.

The aforementioned GA procedure was applied to the design of the piezoelectric panel speaker. The parameters to optimize include the PZT position and the Young's modulus of the panel. The learning curve of the PZT position is shown in Fig. 4(a). With only 5 iterations, the fitness function has converged. From Fig. 4(b), we found the optimal PZT position on the panel to be 1/4 of long side, 1/3 of the short side. On the other hand, the learning

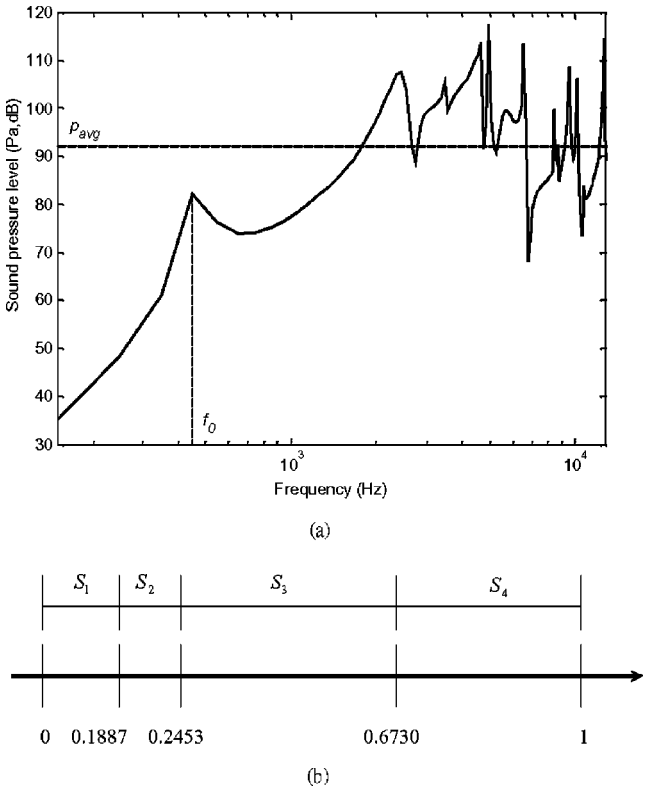

Fig. 3 Pictorial descriptions for optimization of panel speaker design (*a*) frequency response. f_0 is the first resonance frequency greater than 40 dB. p_{avg} is average sound pressure above the frequency f_0 (*b*) the reproduction probabilities of four chromosomes, $c_1 \sim c_4$, with fitness functions, 30, 9, 68, and 52, respectively, concatenated in a real line.

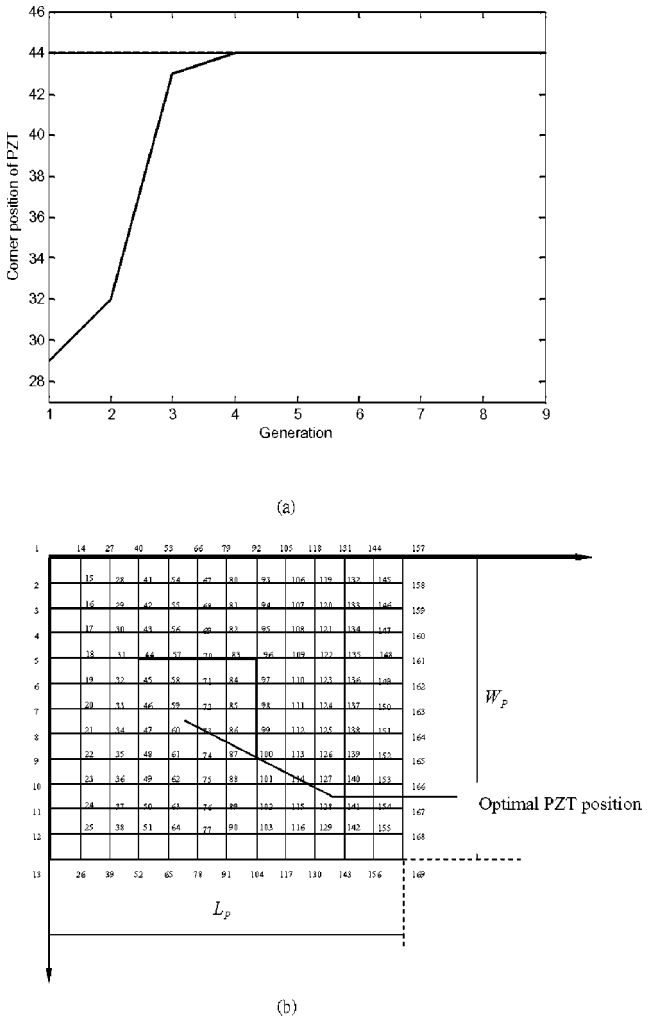

Fig. 4 Optimization of panel speaker design using GA (*a*) the learning curve of the position of PZT. The result has converged within about 5 iterations. (*b*) The optimal position of PZT found by GA.

curve of the Young's modulus of the panel is shown in Fig. 5. The optimal Young's modulus is found within approximately 6 iterations. Similarly, the optimal Young's modulus of the panel is found to be 1.48 GPa.

In addition, the Taguchi method was used again to reach a final design. The dimensions of the panel are 35 mm×25 mm ×0.1 mm, which are close to those of a mobile phone. The parameters to optimize are the PZT shape, panel material, damping, perforation of cabinet and suspension. The results are summarized in Table 3. From Table 3(*a*), the optimal design was found to be: PZT shape is a rectangular plate (2 cm×2 cm or 1.5 cm×3 cm) or a circular disk with radius 1 cm, treated with damping, carbon fiber (0°, 90°), no perforation, and long side suspended. Similarly, from Table 3(*b*), the optimal design was found to be: carbon fiber (0°, 90°), PZT shape is rectangular (1.5 cm×3 cm), treated with damping, no perforation, and suspended with foam material.

4 Numerical Simulation and Experimental Investigations

In this section, numerical simulations and the experimental investigations were undertaken to verify the proposed optimal designs of the piezoelectric panel speaker. The piezoelectric panel speakers are embedded in a baffle while testing and measured in an anechoic room. The implemented piezoelectric panel speaker and experimental arrangement are shown in Fig. 6. The relevant data of the PZT and the panel are summarized in Table 4. The piezoelectric panel speaker implemented on a practical mobile phone is also shown in Fig. 7.

4.1 Frequency Response of On-axis Sound Pressure. The on-axis pressure at 0.5 m from the baffled piezoelectric panel speaker was measured. Random signal of 30 Vrms, band-limited to 12.8 kHz was used as the input. This input voltage level may look higher than the input level used in common voice-coil loudspeakers. This is due to the high input capacitive impedance of the PZT, where a high voltage but small current driver is generally required. Thus, a DC-DC converter is needed to boost the battery voltage to the required level. Based on Eqs. (24) and (25), the frequency responses obtained from experiment and the simulation are compared in Fig. 8, where the condition of damping is assumed as $\alpha=150, \beta=10^{-6}$. The results of the piezoelectric panel speaker model are in reasonable agreement with the experiment in terms of gain level and the first resonance. The discrepancy of the second resonance could be due to mismatch of boundary conditions and material constants between the numerical simulation and the experiment. In particular, the effective stiffness and damping at the suspension is very difficult to model. This could contribute to the errors in the frequency response at high order modes.

Using the FEM model as a simulation platform and Taguchi/GA as an optimization tool, we further examine the design configurations that maximize the ratio of average gain level and the fundamental frequency. Figure 9 shows the effect of the PZT positions. The optimal design (PZT at 1/4 of long side, 1/3 of the short side, as shown in Fig. 4(*b*)) results in $f_0=232$ Hz, $p_{avg}=68.55$ dB,

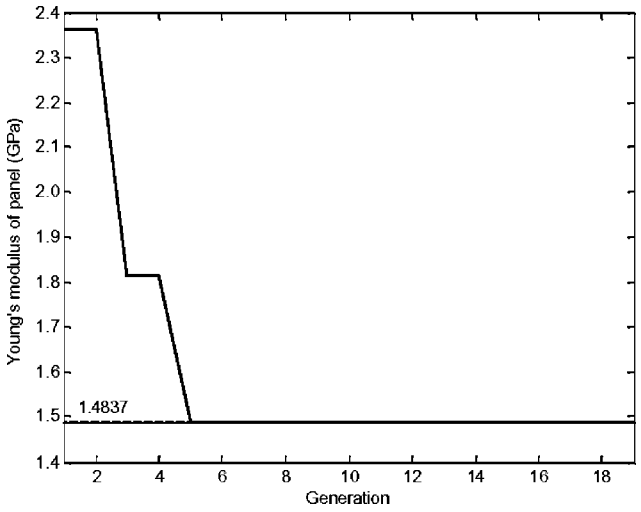

Fig. 5 The learning curve of the optimal Young's modulus of panel. The result has converged within about 6 iterations.

which amounts to the cost function 0.30, while a non-optimal design (PZT mounted at the center) results in $f_0=266$ Hz, $p_{avg}=67.26$ dB, which amounts to the cost function 0.25. The design at the optimal position of the PZT performed better than using a non-optimal one. The first fundamental resonance frequency of the optimal position reduces to approximately 50 Hz. In Fig. 10, the frequency responses of the piezoelectric panel speakers are compared for two panel materials with different Young's modulus. The Young's modulus of the PC panel is 2.7 GPa, which is close to the optimal value obtained from the GA. This nearly optimal design results in $f_0=240$ Hz, $p_{avg}=80.61$ dB, which amounts to the cost function 0.34, while a non-optimal design (copper) results in $f_0=224$ Hz, $p_{avg}=66.21$ dB, which amounts to the cost function 0.29. The sound pressure level produced by the PC panel is about 14 dB higher than that produced by the non-optimal copper panel.

4.2 Sensitivity. Sensitivity was also employed as a performance index in this paper. The input signal is the random noise of 30 Vrms, band-limited to 12.8 kHz. The relevant data of the panel speakers are listed in Table 5. Sound pressure level was measured on-axis at the distance 0.5 m from the source, under the free-field condition. With 0.117 W input electric power, the sensitivity of Speaker1 measured 88.3 dB. The same measurement was repeated for another panel speaker driven by a different PZT material. With 0.078 W input electric power, the sensitivity of Speaker2 measured only 80.2 dB. These results suggest a higher piezoelectric coefficient (h_{31}) leads to higher sensitivity.

4.3 Efficiency. The efficiency is defined as the ratio of the radiated acoustical power to the input electrical power. The input electrical power is calculated according to

$$W_{in}\approx\frac{1}{2}\sum_{i=1}^{N}E[|V_i|^2]\frac{\mathrm{Re}(Z_i)}{|Z_i|^2}\Delta f=\frac{1}{2}\sum_{i=1}^{N}P_{vvi}\,\mathrm{Re}\left(\frac{1}{Z_i}\right)\Delta f \tag{30}$$

where N is number of frequencies, V_i and Z_i are the Fourier transforms of the input voltage and the electrical impedance at the ith frequency, $E[.]$ is the expectation operator, and P_{vvi} is the power spectral density of the input voltage at the ith frequency.

Table 3 The optimal configurations determined by the Taguchi method for a GA session

Factor	Level							
	The f_t of each level							
A (PZT shape)	1		2		3		4	
	Disk ($r=1$ cm)		Plate (1 cm×1 cm)		Plate (2 cm×2 cm)		Plate (1.5 cm×3 cm)	
	0.4054		0.0771		0.4478		0.5008	
B (Damping)	With damping		Without damping					
	0.4964		0.2192					
C (Panel material)	Carbon fiber (0°,0°)		Carbon fiber (0°,90°)					
(Thickness=0.1 mm)	0.3036		0.4119					
D (Perforation)	Perforation		No perforation					
	0.2550		0.4605					
E (Suspension)	Long side suspended		Short side suspended					
	0.4965		0.2190					
Run	1	2	3	4	5	6	7	8
f (Hz)	1200	700	2000	2200	500	1600	1200	3000
p_{avg} (dB)	70	60	62	50	60	72	75	60
Factor	Level							
	The f_t of each level							
A (Panel material)	1		2		3		4	
(Thickness=0.1 mm)	Laminate		Carbon fiber (0°,90°)		Carbon fiber (0°,0°)		Copper	
	0.2127		1.4561		0.9592		0.9930	
B (PZT shape)	Plate (1.5 cm×3 cm)		Plate (2 cm×2 cm)					
	0.7107		1.0998					
C (Damping)	Without damping		With damping					
	0.5873		1.2231					
D (Perforation)	Perforation		No perforation					
	0.7845		1.0260					
E (Suspension)	White foam		Black foam					
	1.5516		0.2589					
Run	1	2	3	4	5	6	7	8
f_0 (Hz)	1400	1000	1900	800	2000	700	750	2450
p_{avg} (dB)	64	60	72	80	70	75	77	62

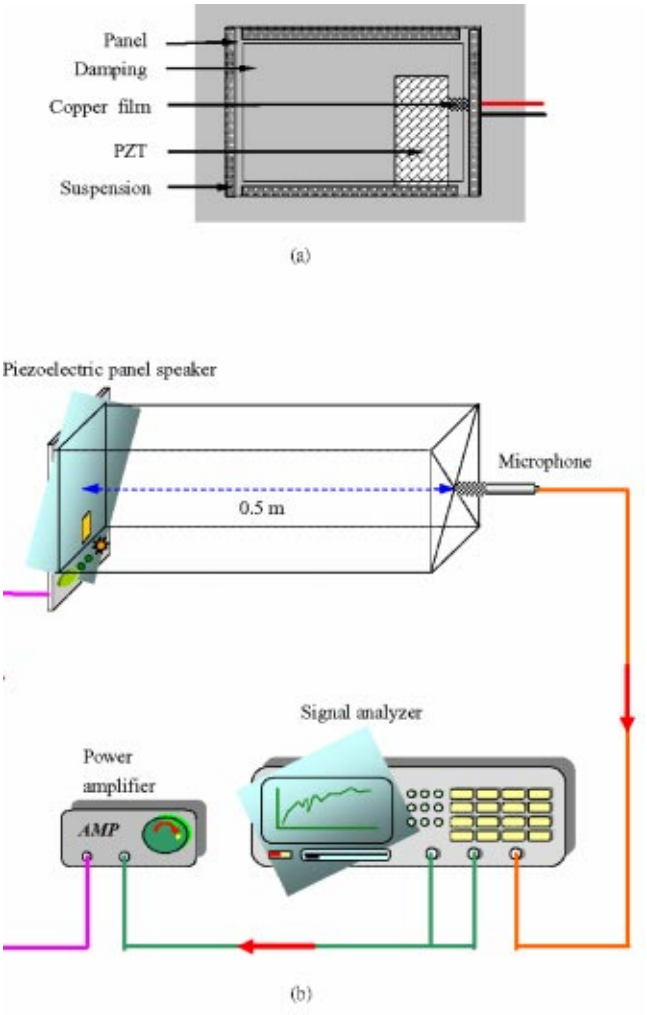

Fig. 6 Experimental arrangement of the piezoelectric panel speaker (*a*) physical construction of the piezoelectric panel speaker (*b*) the experimental setup for the performance measurement.

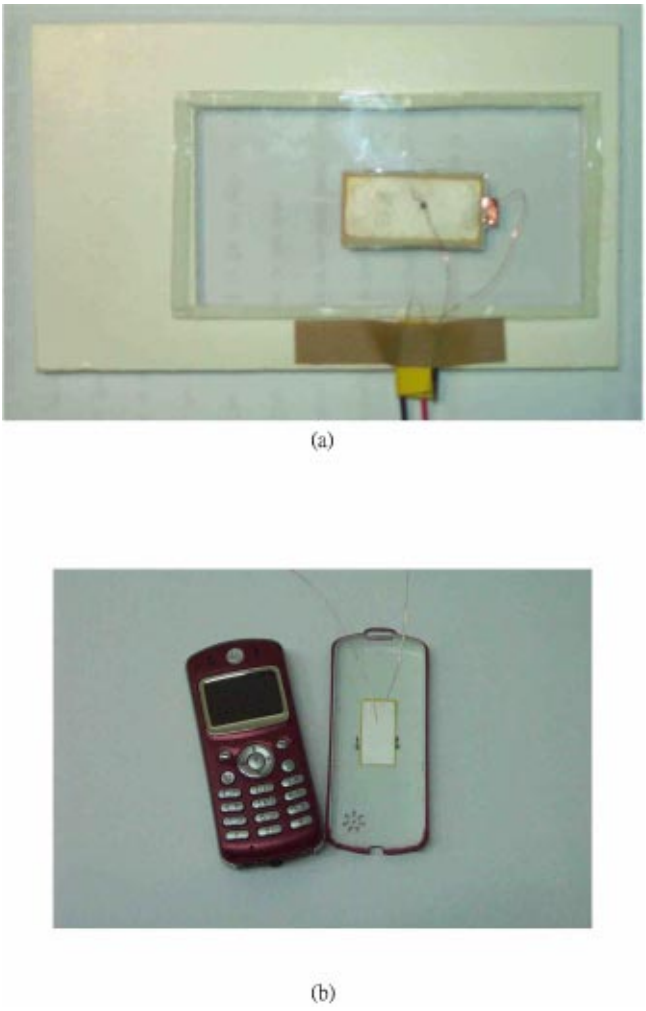

Fig. 7 Photos of piezoelectric panel speakers (*a*) a baffled piezoelectric panel speaker. The panel material is transparent PC. (*b*) A piezoelectric panel speaker implemented on a mobile phone.

In this work, ISO 3745 was employed for measuring the radiated sound power in the anechoic room [11]. The measured efficiency of the Speakers 1, 2 and 5 were $\eta = 0.76\%$, 0.56% and 0.78%, respectively. As expected, the material with a higher piezoelectric coefficient (h_{31}) produced higher efficiency. For reference, the efficiency of a panel speaker driven by a voice-coil

Table 4 Relevant data of the PZT and the panel used in the simulation and experiments, to verify the FEM model. Dimensions of the piezoelectric panel speaker are 60 mm×60 mm ×0.3 mm.

	Parameter	Value
Aluminum plate	size	60 mm×60 mm×0.2 mm
	density	2790 kg/m^3
	Young's modulus	73.1 GPa
	Poisson's ratio	0.33
PZT	size	20 mm×20 mm×0.1 mm
	β_{33}^S	2.3077×10^7
	h_{31}	-3.21×10^8 V/m
	c_{11}^D	23.16×10^{10} N/m^2
	c_{12}^D	14.07×10^{10} N/m^2
	c_{66}^D	4.545×10^{10} N/m^2

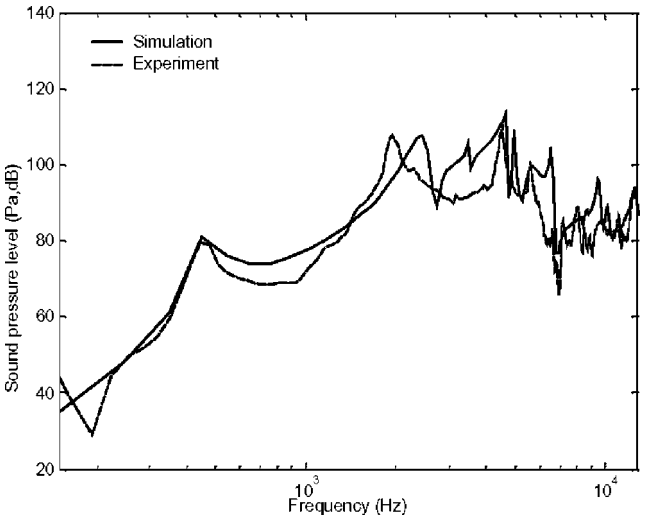

Fig. 8 Comparison of the on-axis pressure response of the FEM simulation and the measurement

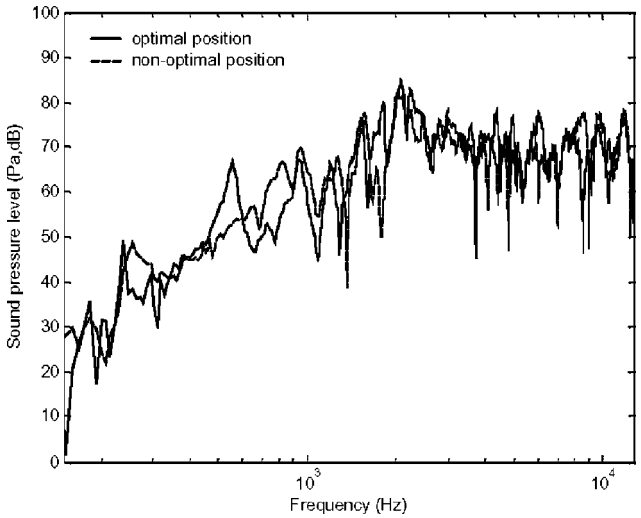

Fig. 9 On-axis pressure response responses of the piezoelectric panel speaker are compared for an optimal design obtained using GA and a non-optimal position

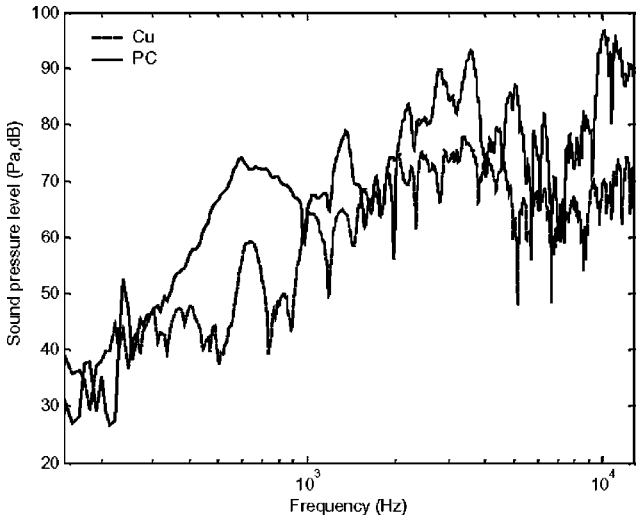

Fig. 10 Frequency responses of the piezoelectric panel speaker. The effect of Young's modulus of panel is investigated. The Young's modulus of the PC panel is close to the optimal value obtained from the GA procedure

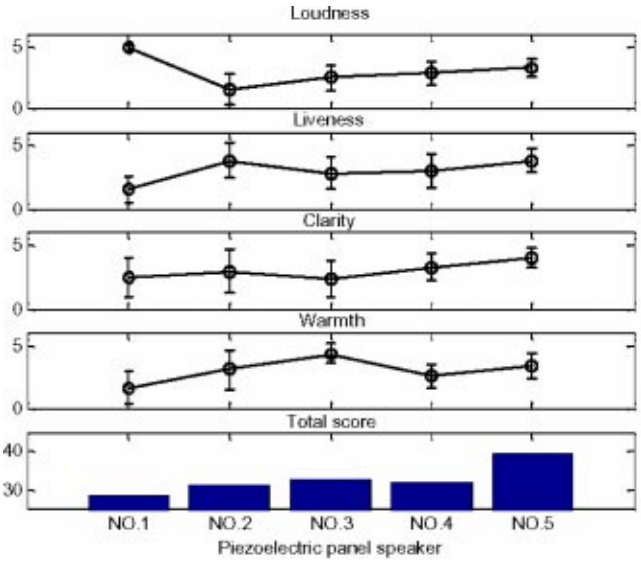

Fig. 11 Results of the subjective listening test for the music input. Five configurations of piezoelectric panel speakers are compared. The average and spread of test result are indicated on the figure

exciter was found to be 0.075%, which is almost one order less than the piezoelectric counter part. This indicates that piezoelectric panel speakers are very efficient and well suited for many battery-powered devices.

4.4 Subjective Listening Test. As mentioned previously, one of the goals of the present study is to enhance the piezoelectric device to a level for audio purpose. Therefore, subjective listening test were carried out to assess the audio quality delivered by the piezoelectric panel speakers. Five kinds of piezoelectric panel speakers, listed in Table 6, were used in the listening test. Four subjective indices, loudness, clarity, liveness, and warmth are employed in the test. Specically, ''clarity'' is intelligibility of audio signal, ''naturalness'' is the fluidity of rendering, ''liveness'' is the middle and high frequency reverberation (500 Hz $\sim$2 kHz), and ''warmth'' is the low frequency reverberation (less than 500 Hz) [12]. There were eleven subjects taking part in the listening test. All of these subjects listened to a segment of music and another segment of speech. The results of listening test are shown in Figs. 11 and 12. It was found that the speaker No. 1 produced the highest loudness, but the worst performance in the

Table 5 Relevant data of the PZT and the panel for two panel speaker configurations, used in the simulation and experiments. Dimensions of the piezoelectric panel speaker are 60 mm×60 mm×0.3 mm

	Speaker1	Speaker2
Panel size	42 mm×84 mm×0.1 mm	42 mm×84 mm×0.1 mm
Panel material	Carbon fiber	Carbon fiber
Boundary condition	White foam	White foam
PZT size	15 mm×30 mm×0.1 mm	15 mm×30 mm×0.1 mm
PZT position	1/4 of long side, 1/3 of short side	1/4 of long side, 1/3 of short side
c_{11}^D	23.16×10^{10} N/m^2	11.73×10^{10} N/m^2
c_{12}^D	14.07×10^{10} N/m^2	7.77×10^{10} N/m^2
c_{66}^D	4.545×10^{10} N/m^2	1.98×10^{10} N/m^2
h_{31}	-3.21×10^8 V/m	-8.1×10^8 V/m
β_{33}^S	2.3077×10^7	1.94×10^8

Table 6 Five configurations of piezoelectric panel speaker used for a subjective listening test. The dimensions of the panel speaker are 42 mm×84 mm×0.1 mm. The PZT is the same as that used in Speaker 1 of Table 5

Speaker number	Panel material	Panel size (mm)	PZT size (mm)	PZT position (mm)	Boundary condition
No.1	Carbon fiber	42×84×0.1	15×30×0.1	(14,21)	White foam
No.2	PC	42×84×0.1	15×30×0.1	(14,21)	White foam
No.3	Laminate	42×84×0.1	15×30×0.1	(14,21)	White foam
No.4	Carbon fiber+ damping	42×84×0.1	15×30×0.1	(14,21)	White foam
No.5	Acrylic fiber	42×84×0.1	15×30×0.1	(14,21)	White foam

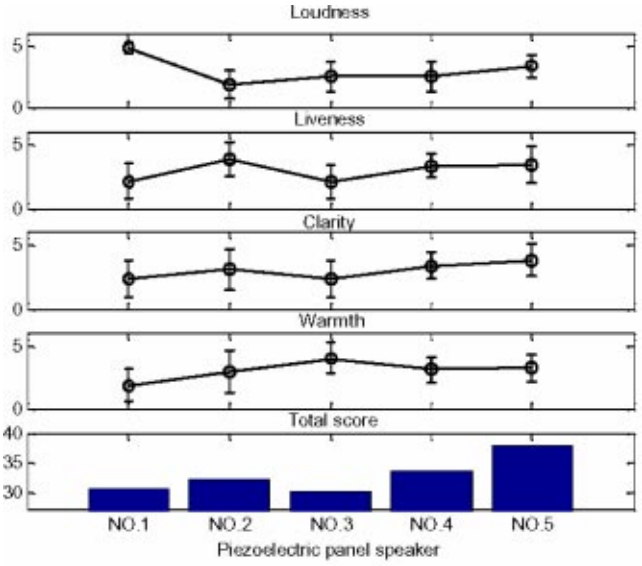

Fig. 12 Results of the subjective listening test for the speech input. Five configurations of piezoelectric panel speakers are compared. The average and spread of test result are indicated on the figure.

other indices (total score=29 and 31, respectively, for music and speech listening). On the other hand, the panel speaker No. 5 appears overall the best piezoelectric panel speaker for both music and speech listening (total score=40 and 38, respectively).

5 Conclusions

Optimal design and implementation of miniature piezoelectric panel speakers have been presented in this paper. A FEM-based model has been developed to serve as the simulation platform. Optimal designs have been obtained with the aid of the Taguchi method and GA method. The Taguchi method is intended for the preliminary search of optimal configuration and experimental design. The GA method proves effective in fine-tuning the design parameters. Based on these two methods, an optimal design methodology for piezoelectric panel speakers is presented in this paper. The performance and adequacy as a broadband loudspeaker of the proposed device is investigated. As confirmed by the numerical and experiment results of various indices, the piezoelectric panel speaker using the optimal configuration indeed produced better performance than the non-optimal ones.

From the experimental results, the advantages of the piezoelectric panel speaker are two-fold. The piezoelectric panel speaker achieves an impressive efficiency (approximately 10:1) over the voice-coil driven counterpart. In addition, the thickness of piezoelectric panel speaker measures only 0.2 mm, which is also much less than the 2.4 mm of the voice-coil counterpart. Overall, the piezoelectric panel speaker has displayed the potential for the 3C applications.

Acknowledgments

Thanks are due to the illuminating discussions with NXT, New Transducers Ltd, UK. The work was supported by the Nation Science Council in Taiwan, Republic of China, under the project number NSC 91-2212-E009-032.

References

[1] Bai, M. R., and Huang, T., 2001, ''Development of Panel Loudspeaker System: Design, Evaluation and Enhancement,'' J. Acoust. Soc. Am., **109**, pp. 2751–2761.
[2] Azima, H., 1998, ''NXT, Up Against Wall,'' Audio Magazine, September, pp. 34–41.
[3] Waanders, J. W., 1991, *Piezoelectric Ceramics Properties and Applications*, Philips Components, Eindhoven.
[4] Langhaar, H. L., 1962, *Energy Methods in Applied Mechanics*, John Wiley and Sons, New York.
[5] Tiersten, H. F., 1969, *Linear Piezoelectric Plate Vibration*, Plenum press, New York.
[6] Davis, C. R., 1989, *Concepts and Applications of Finite Element Analysis*, John Wiley and Sons, New York.
[7] Berkhoff, A. P., 2000, ''Sensor Scheme Design for Active Structural Acoustic Control,'' J. Acoust. Soc. Am., **108**, pp. 1037–1045.
[8] Meirovitch, L., 1986, *Elements of Vibration Analysis*, McGraw-Hill, Singapore.
[9] Hicks, C. R., and Turner, K. V., 1999, *Fundamental Concepts in the Design of Experiments*, Oxford University Press, New York.
[10] Holland, J. H., 1962, ''Outline for a Logical Theory of Adaptive System,'' J. Assoc. Comput. Mach., **3**, pp. 297–314.
[11] Turner, J. D., and Prtylove, A. J., 1991, *Acoustics for Engineers*, McMillan Education, New York.
[12] Zwicker, E., and Fastl, H., 1999, *Psycho-acoustics: Fact and Models*, Springer-Verlag, New York.